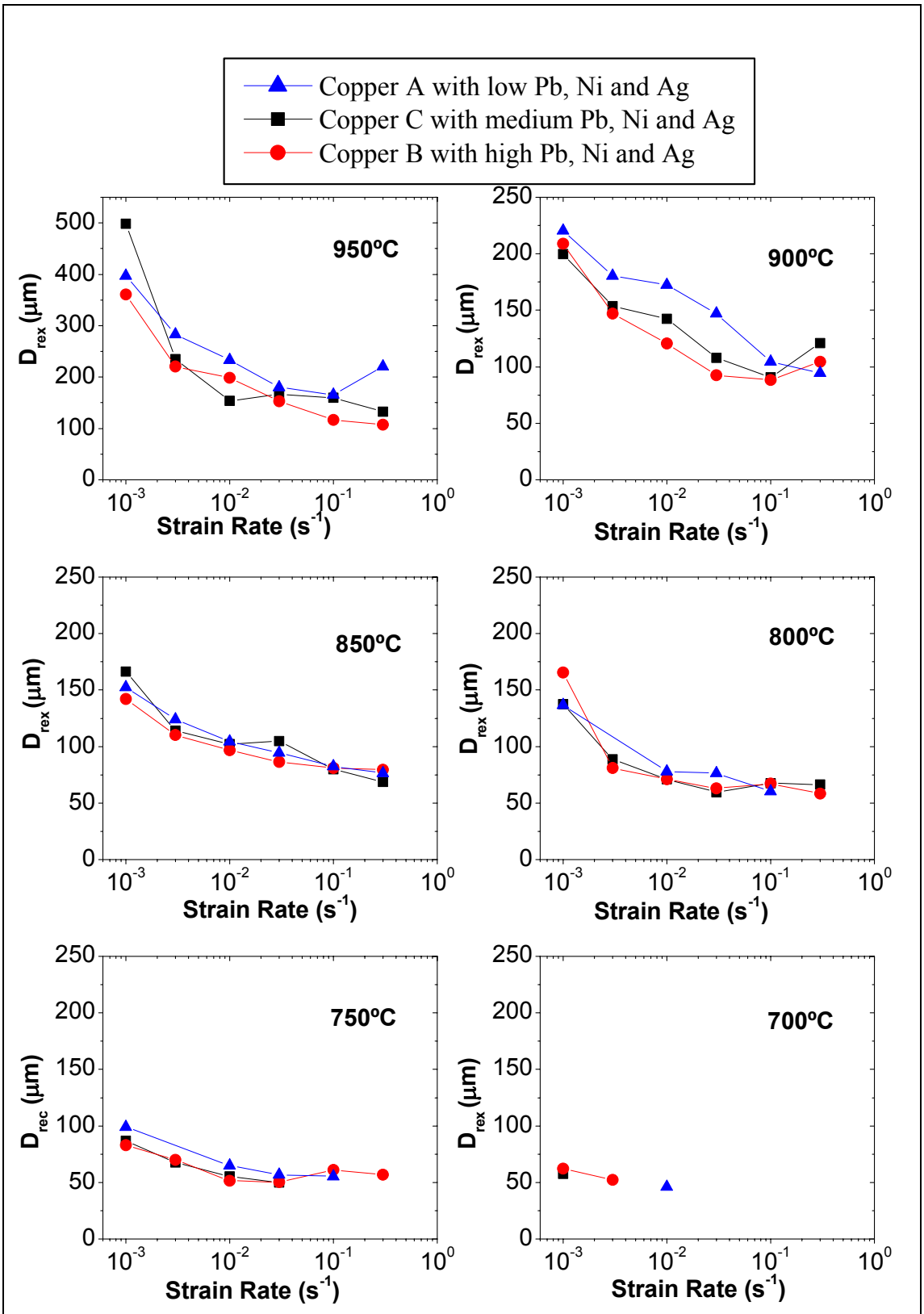

Fig. 3.46 Comparison of the dynamically recrystallized grain diameters between Cu A, B and C at different temperatures. At lower temperatures only incomplete DRX was found. Notice that the scale of the plot at 950 is more than double of the rest.

3.3 Grain Growth Studies

The grain growth studies of Cu A [8] and Cu C demonstrate the rate of static growth of the as-received material at the temperatures employed on earlier hot compression tests. The static grain growth rate is probably slower than a dynamical growth rate, but a minimum estimate of how fast a grain grows was obtained. Also undoubtedly post dynamical grain growth occurred in the few instants between the hot compression test and the quenching. A grain growth study helps to understand how the latter post dynamical grain growth might have affected the observed grain on the final microstructure. The plot by Rius et al. [8] on fig. 3.47 shows a grain diameter growth versus time inside the oven of Cu A performed at 950ºC, 900ºC, 850ºC and 800ºC. The scale of the study was conveniently separated to appreciate the behavior at lower temperatures thus on fig. 3.48 the plot at 750ºC, 700ºC, 650ºC and 600ºC is presented.

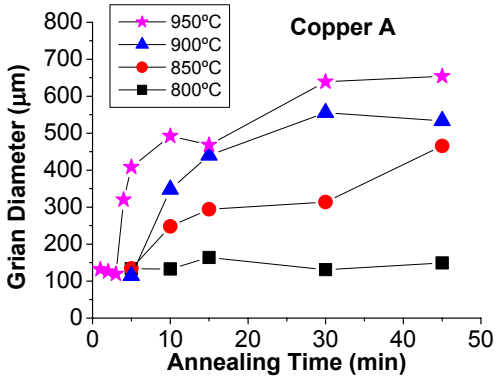

Fig. 3.47 Grain growths of Cu A between 800ºC and 950ºC. Twin boundaries were not included.

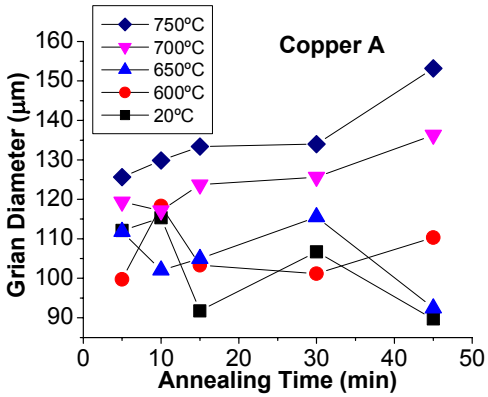

Fig. 3.48 Grain growths of Cu A between 600ºC and 750ºC. Twin boundaries were not included. Initial grain at 20ºC is reported.

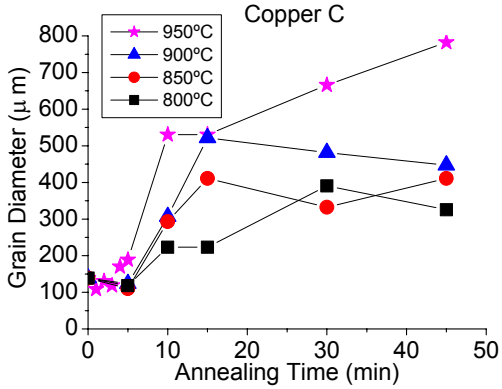

Fig. 3.49 Grain growths of Cu C between 800ºC and 950ºC. Twin boundaries were not included.

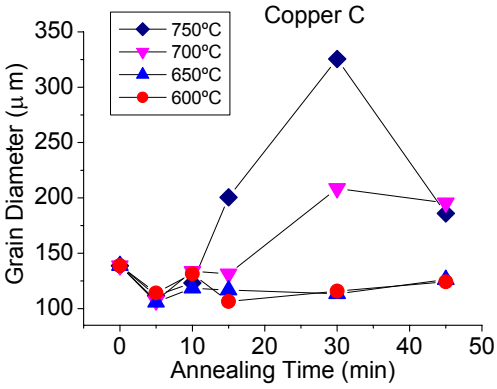

Fig. 3.50 Grain growths of Cu A between 600ºC and 750ºC. Twin boundaries were not included. Initial grain at 20ºC is reported.

As means of having a controlled sample, which showed the initial grain size variation, un-annealed samples labeled 20ºC were also included in the plot of fig. 3.48. As expected the plot (800º-950ºC) on fig. 3.47 shows that at higher annealing temperatures the initial grain grew more for the same amount of time. Also a stable grain size after impingement was expected, but such stable grain size could only be seen after 30 minutes annealing for the 900ºC and 950ºC lines. The scale of fig. 3.47 also shows that below 800ºC grain growth is slow for the as received copper A. The plot on fig. 3.48 with a smaller scale shows that an activation energy requirement to begin growth was achieved at a minimum temperature of 700ºC and 10 minutes annealing time. At lower temperatures the time requirement to observe growth is larger than the scope of the experiment. Figures 3.47 and 3.48 show how the as received grain size of Cu A, which is the purest and of lowest oxygen content, would grow if subjected to several annealing temperatures.

The grain growth behavior of the three coppers of this study was thought to be different however how much different was unknown hence for comparison purposes grain growth studies with the other coppers were performed. A grain growth study for Cu C is presented in figures 3.49 and 3.50. As before fig. 3.49 shows at a larger scale the grain growth behavior from 800ºC to 950ºC. Some data points cross implying inevitable experimental error, however the tendency is the same as earlier with Cu A where a higher annealing temperature made the initial grain size grow more for the same amount of time. At lower temperatures (600º-750ºC) the plot on fig. 3.50 a smaller scale was employed, but notice that the scale is larger than the one needed for Cu A in fig. 3.48. From fig. 3.50 on can point out that the minimum temperature and time needed to observe grain growth was 700ºC and 15 minutes for Cu C, unlike the 10 minutes for Cu A. Also once growth started for Cu C the rate seemed higher than in Cu A, if fig. 3.48 and 3.50 are compared. In general the plots on figures 3.47 through 3.50 show that a higher temperature makes the as received grain grow faster, however other plots are necessary for comparison purposes.

The comparative plots between Cu A and Cu C at equal temperatures on fig. 3.51 showed that the grain growth rate is similar on both coppers, however some differences can be pointed out. The plots at 950ºC through 800ºC on fig. 3.51 show that for short periods of time Cu C grows at a slower rate than Cu A, however suddenly at around 5 to 10 minutes growth lines cross and Cu C grows faster than Cu A. On the 800ºC plot a decrease of Cu C after 15 minutes was measured, which could only be attributed to inherent experimental error while counting large grains. As explained the main difference between Cu A and Cu C is the oxygen content. The delayed and then sudden growth of Cu C can be explained through a pinning effect on the grain boundaries by a higher volume fraction of copper-oxide particles in Cu C. After some time the pinned grain boundaries burst due to the increased difference in stored energy, which causes a faster grain growth effect. Regarding the influence the difference in growth behavior may have had on the quenched final microstructure then one can state that only the slowest compression test at $0.001s^{-1}$ exceeded the 5 to 10 minutes when the growth appeared to be different. The time, t, required for a test is given by $t = 0.8/\dot{\varepsilon}$, where 0.8 is the final strain. A faster growth of Cu C after 5 to 10 minutes means that the dynamically recrystallized grain diameter seen on fig. 3.46 might have been harder to retain during the quenching procedure. No further inquiries about the differences in grain growth were sought, because drawing firm conclusions of how a static growth study influenced a dynamic process needed a separate and more controlled investigation.

The summarizing observation drawn from this particular study is that the grain growth kinetics of coppers A and C are similar, however due to a higher volume fraction of particles Cu C started to grow at a higher rate at around 5 to 10 minutes, which is an effect more noticeable the higher the temperature. The assumption that the dynamically recrystallized grain during hot compression tests grows in the same manner as the growth observed during static grain growth is not straight forward, because the driving force of new recrystallized grains is higher (the difference of stored energy between both sides of the grain boundary is higher). This grain growth study only gives an idea of the effect different volume fraction of particles can have on grain boundary pinning.

A single comparative plot between Cu A and Cu C at lower temperatures (see fig. 3.52) showed that for 700ºC and 750ºC Cu C grew at a much faster rate than Cu A. The latter behavior was pointed out before when presenting fig. 3.50. The growth studies presented will not be discussed further, because they are only preliminary and served only to answer hypotheses about how difficult would have been to retain the dynamically recrystallized grain size and what should the annealing time be to reach a desired grain size.

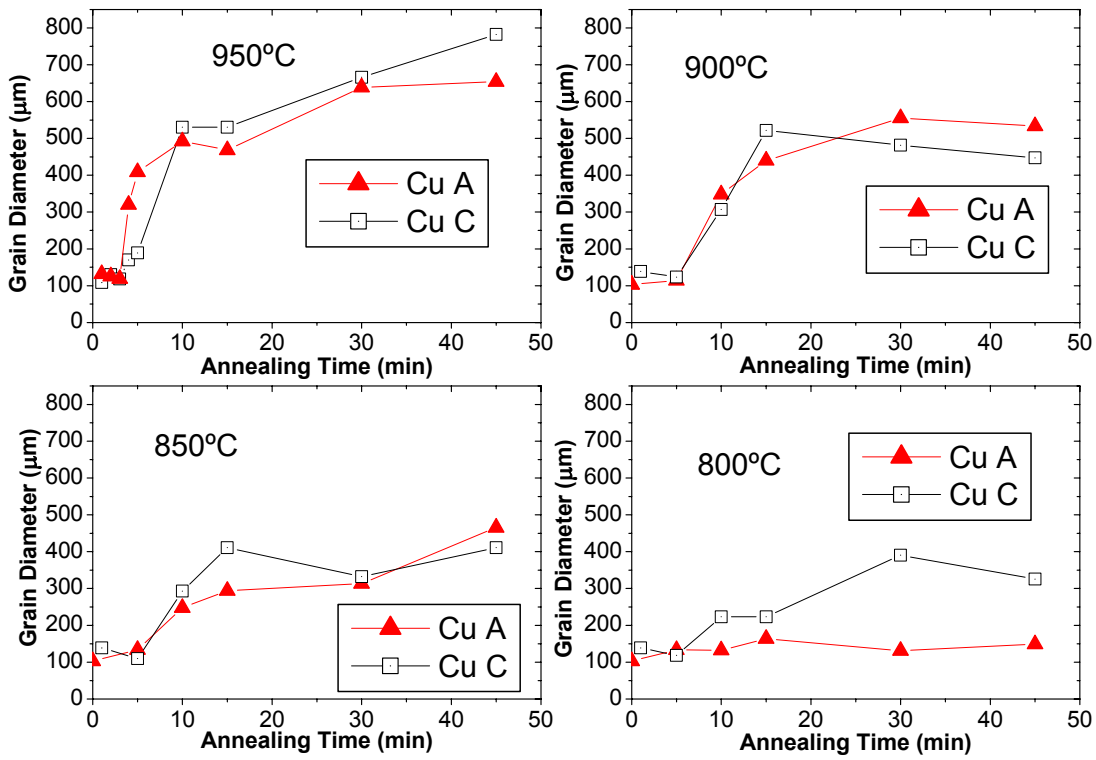

Fig. 3.51 A grain growth comparison between Cu A and Cu C at different temperatures.

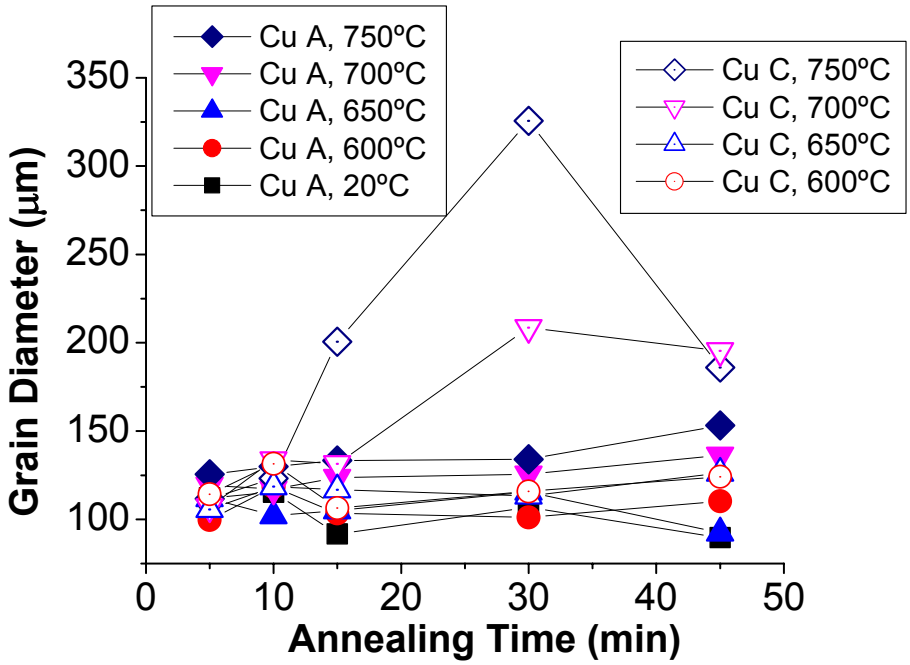

Fig. 3.52 A grain growth comparison at lower temperatures between Cu A and Cu C.

3.4 Inclusions

The hypotheses leading to an inclusion size and distribution determination supposed that inclusions were responsible for the increased strain hardening during warm working temperatures and that the copper with highest oxygen content would have the highest quantity of inclusions. Table 3.1 summarizes the findings of the inclusion investigation. The histograms on figures 3.53, 3.54 and 3.55 show the inclusion size and frequency found on an equal size area of Cu A, Cu B and Cu C respectively. If the information on Table 3.1 is believed as representative of the entire copper microstructure then one may believe that the initial hypotheses are partially true, because Cu C with the highest oxygen content possessed the highest area fraction occupied by inclusions, followed by Cu B and then Cu A, which correlates well with the observed strengthening at warm working temperatures. However when the number of inclusions is examined the order does not correlate in the same manner. Also the size frequency of inclusions does not correlate with the strengthening observed during the hot compression tests. Copper C showed a highest quantity of particles between 0.4μm and 0.5μm. Copper B showed a highest quantity of particles measuring between 0.7μm and 0.8μm. While on Cu A the highest number of particles measured 0.6μm to 0.7μm. A question might be raised on how representative a surveyed area of 184,616.5μm^2 is of a large grained copper. Possibly a higher area may show different results. Edelson and Baldwin [9] studied sintered copper with different particles of different sizes and showed that the size and the volume fraction had to be much higher than the one present on the coppers of this study to have an affect on any fracture mechanisms during tension. The inclusion distribution investigation is non-conclusive, because on one hand the area fraction occupied is as would be expected, but the size distribution do not support a strengthening hypothesis.

Other unexpected findings might be plaguing with experimental error this inclusion investigation. From the histograms one can observe that if the size distributions follow a normal distribution then inclusions below 0.25μm were too small to be recorded. Counting inclusions smaller than 0.25μm over a large area is technically difficult even using Scanning Electron Microscopy. Large inclusions are less frequent in Cu A (see fig. 3.53). However both Cu B and Cu C showed large inclusions nearly 4μm in diameter (see figures 3.54 and 3.55). The latter finding could be fortuitous. However on the three annealed coppers a majority of the inclusions were found on the edge nearest to the cylinder surface. Could inclusions during the annealing treatment have migrated toward the surface and some coalesced to form large inclusions? Figures 3.56, 3.58 and 3.60 show the SEM micrograph surveyed were the largest number of inclusions were found for Cu A, Cu B and Cu C. The X-ray intensity spectrums

Table 3.1. Summary of the number of inclusions found in Cu A, Cu B and Cu C.

	Area Scanned for Inclusions (μm^2)	Area Occupied by Inclusions (μm^2)	Area Fraction Occupied by Inclusions	Number of Inclusions Found
Cu A	184,616.5	54.58417	2.956XE-4	97
Cu B	184,616.5	69.23964	3.750XE-4	68
Cu C	184,616.5	103.48496	5.605XE-4	204

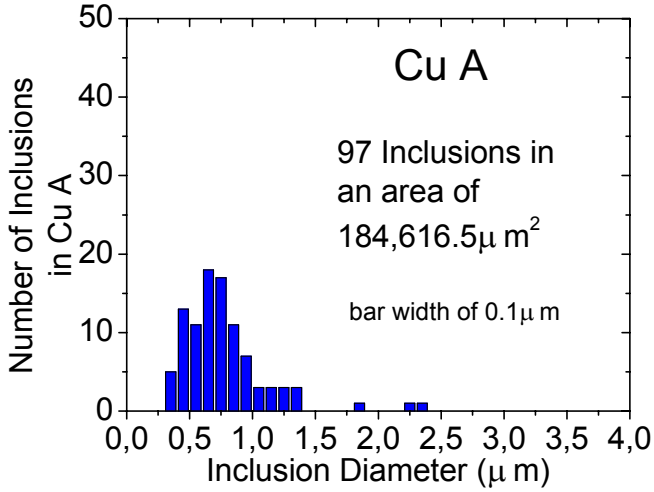

Fig. 3.53 A histogram of the inclusions found on an untested but annealed cylinder of Cu A.

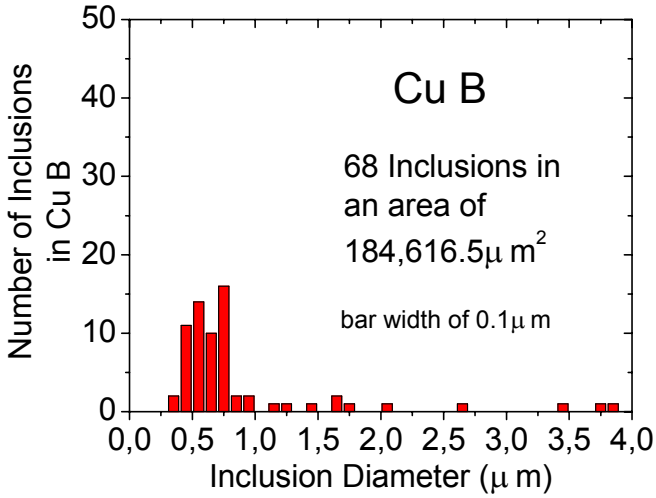

Fig. 3.54 A histogram of the inclusions found on an untested but annealed cylinder of Cu B.

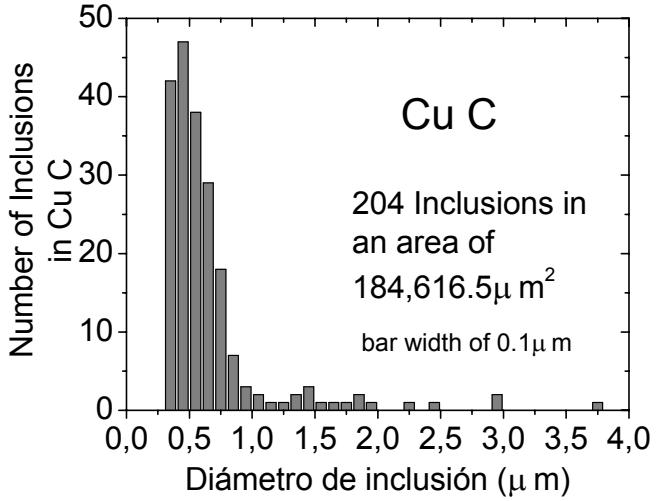

Fig. 3.55 A histogram of the inclusions found on an untested but annealed cylinder of Cu C.

appearing on figures 3.57, 3.59 and 3.61 show the chemical composition of the inclusions for Cu A, Cu B and Cu C respectively. The inclusions on Cu A and Cu B show the presence of O, Fe, P, Pb and Zn besides Cu. The carbon peak appearing on the spectrums cannot be ascertained to originate from the coppers, because during the polishing procedure oil lubricant and diamond paste were used, which contain carbon. The spectrum on fig. 3.61 of inclusions on Cu C, which appear on fig. 3.60 did not show the presence of Zn as did Cu A and Cu B. However the spectrum of an inclusion of the same Cu C on fig. 3.66 did show Zn. The findings of the inclusion investigation indeed raise more questions without completely answering previous ones.

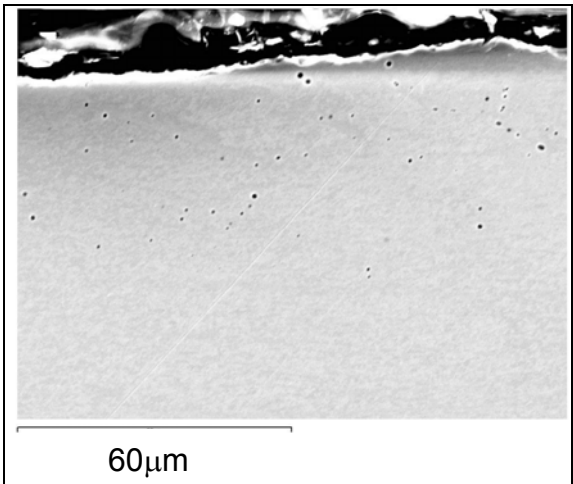

Fig. 3.56 After annealing a majority of the inclusions on Cu A were found on the edge nearest to the surface of the test cylinders.

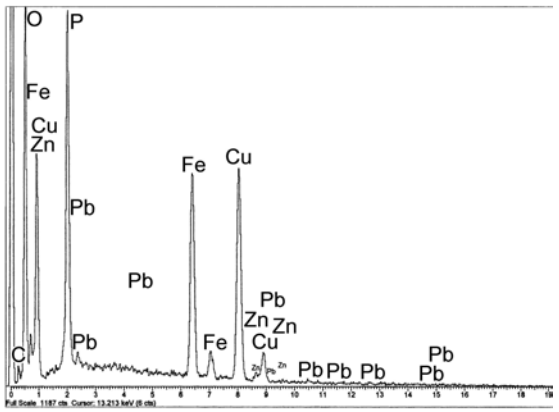

Fig. 3.57 An X-ray intensity spectrum on an inclusion of Cu A shows the presence of O, Fe, P, Pb and Zn besides Cu. The carbon peak could be due to the lubricant and diamond paste used during polishing.

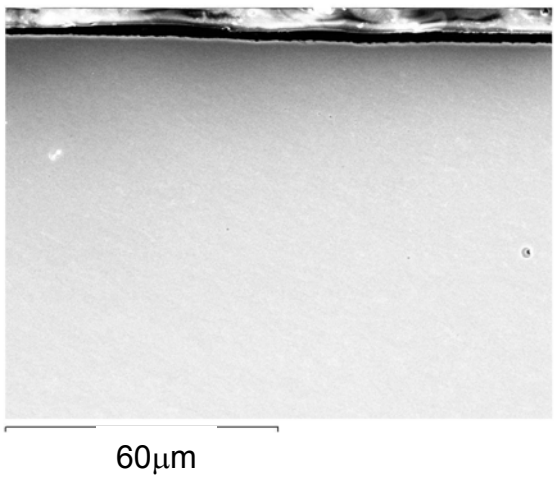

Fig. 3.58 Although small the majority of the inclusions on Cu B were also found on the edge nearest to the surface of the test cylinders.

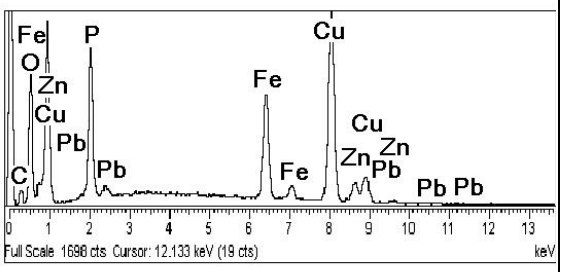

Fig. 3.59 An X-ray intensity spectrum on an inclusion of Cu B shows the presence of O, Fe, P, Pb and Zn besides Cu. The carbon peak could be due to polishing procedure.

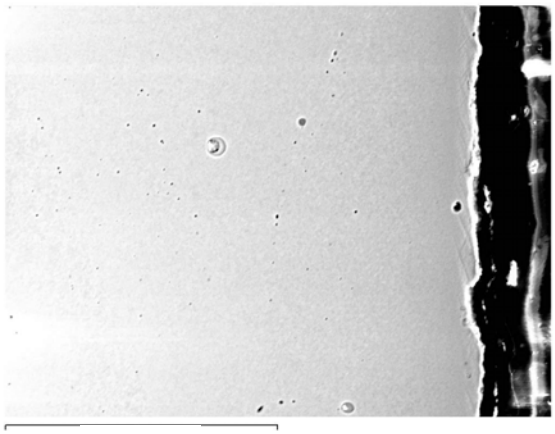

Fig. 3.60 The majority of the inclusions on Cu C were also found on the edge nearest to the surface of the test cylinders.

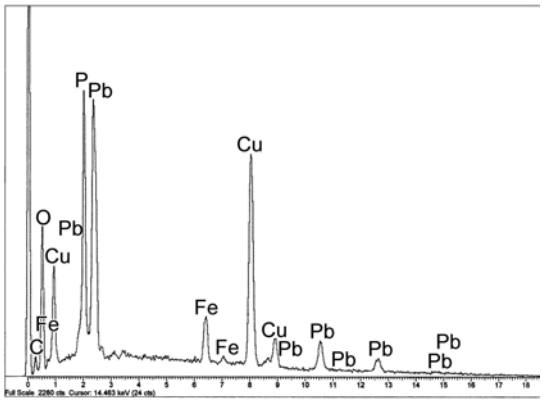

Fig. 3.61 An X-ray intensity spectrum on an inclusion of Cu C shows the presence of O, Fe, P and Pb besides Cu. The carbon peak could be due to polishing procedure.

One other important matter concerning inclusions is their influence on the microstructure of the hot compressed copper samples. A search for inclusions on samples compressed at lower temperatures is seen on fig. 3.62 where a SEM micrograph after 600ºC, $0.3s^{-1}$ and 0.8 of strain shows flattened initial grains and some dynamically recrystallized grains. A zoom of the previous micrograph shows flattened holes, which contained inclusions (during the polishing procedure the 1μm diamond paste makes inclusions jump out). A greater zoom of fig. 3.63 seen on fig. 3.64 shows two holes where inclusions laid and one of them has a recrystallized grain around. Caution should be taken before stating that inclusions help nucleate grains during dynamic recrystallization, because the new grain observed on fig. 3.64 could have recrystallized meta-dynamically, after the compression test. Another recrystallized grain associated to an inclusion is seen on fig. 3.65 also from Cu C after 600ºC, $0.3s^{-1}$ and 0.8 of strain. The X-ray intensity spectrum corresponding to fig. 3.65 is seen on fig. 3.66. One observation is clear; inclusions help nucleate new grains either during DRX or meta-DRX. If recrystallization takes place after compression then figures 3.64 and 3.65 could be another example of Particle Stimulated Nucleation (PSN). The implications of having more inclusions could be a finer microstructure, which may improve mechanical properties if inclusions are not too abundant (inclusions are deleterious for mechanical properties). Regarding the three coppers under study, a higher inclusion number on Cu C should have produced a finer grain size, however that was not the case; instead Cu B produced a statistically finer grain size. The inclusion content remained an open question and answers to the observed strengthening during warm working temperatures were found while searching for precipitates, which is the next subject that will be presented.

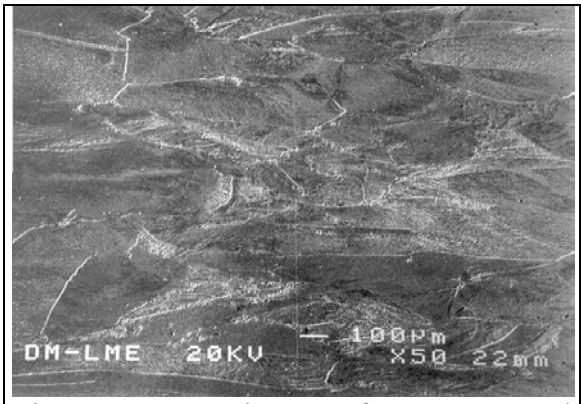

Fig. 3.62 SEM image of a compressed sample of Cu C after 600ºC, $0.3s^{-1}$ and ε = 0.8.

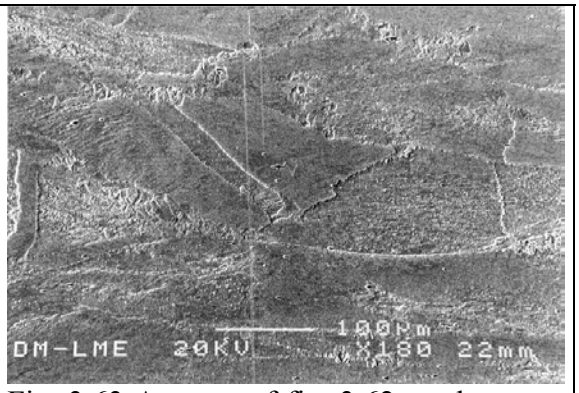

Fig. 3.63 A zoom of fig. 3.62 to observe a compressed inclusion within a grain.

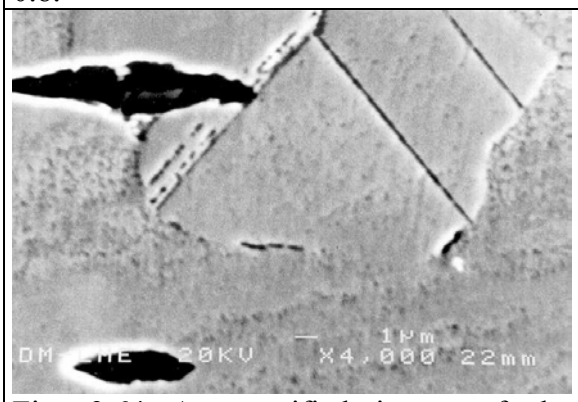

Fig. 3.64 A magnified image of the compressed inclusion appearing on fig. 3.63. A new grain surrounds part of the inclusion.

Fig. 3.65 On the same sample as in fig. 3.62 another compressed inclusion surrounded by a new grain was found.

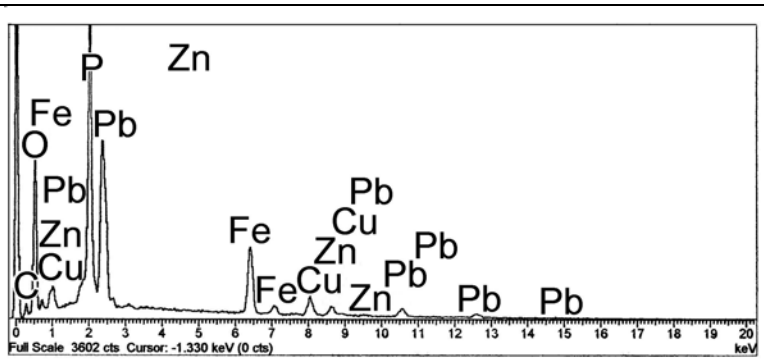

Fig. 3.66 An X-ray intensity spectrum of the compressed inclusion on fig. 3.65 indicates the presence of O, Fe, Zn, Pb and P. The presence of Cu was expected however the C peak might be due to the lubricant and diamond paste used during the polishing procedure.

3.5 Transmission Electron Microscopy

Convincing proof of the existence of fine precipitates was only found in the samples of Coppers B and C and only after 750ºC. Rather large particles (33-300nm) were found on Copper A regardless of the electrolyte employed to thin the samples. Figures 3.67 and 3.68 show the TEM images of the large particles found in Cu A while employing the electrolyte containing nitric acid, which was the electrolyte that seemed to create a debris free surface. In any case these large particles were found in sparse quantities and, if they truly belong to the original fire-refined copper they would be too large to strengthen the matrix, as will be explained later. When using the electrolyte containing nitric acid for the samples compressed at 900ºC no precipitates or particles were found.

The nitric acid electrolyte appeared to be more reliable, however the samples in which precipitates were found presented a technical difficulty in that no temperature or voltage seemed to produce a foil with a smooth thickness. An example of the foils where precipitates were found is seen on figures 3.69 and 3.70 of Cu B after 750ºC, $0.3s^{-1}$ and 0.8 of strain. The transmission micrograph on fig. 3.69 shows a bright field image of a grid like or flaky surface, but a dark field image on fig. 3.70 outlines the grid with small bright points, which correspond to precipitates. The grid like pattern was

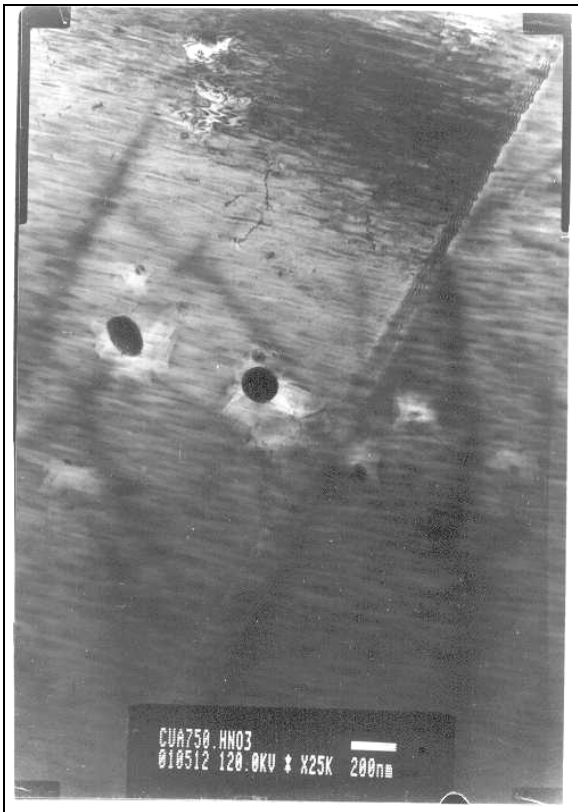

Fig. 3.67 The TEM image above shows some of the few large particles found on Cu A after 750ºC, $0.3s^{-1}$ and ε = 0.8. However most of Cu A was found to be free of particles.

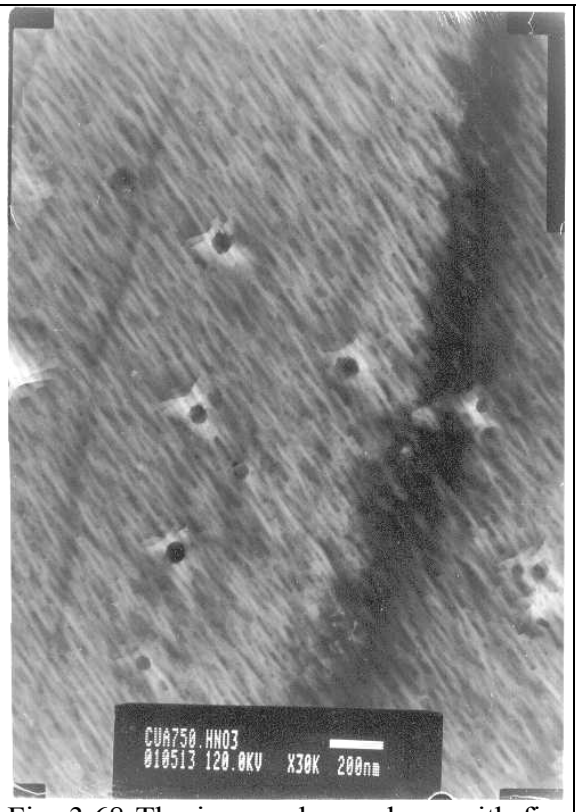

Fig. 3.68 The image above along with fig. 3.67 constitute the only particles found on Cu A using a nitric acid electrolyte.

found to have several sizes. Another transmission micrograph of Cu B appearing on fig. 3.71 shows a slightly different shape of the described pattern adopted by the precipitates. Figures 3.72 and 3.73 show the bright field and dark field images of Cu C after 750ºC that also reveal the existence of precipitates on the copper with highest oxygen content. The precipitates on fig. 3.73 do not arrange themselves in any clear pattern. Figures 3.74 and 3.75 are a zoom of figures 3.72 and 3.73 respectively. The TEM images helped to demonstrate the existence of fine crystallites, which could be serving as effective obstacles to dislocation motion and consequently raising the flow stress, however evidence of pinned dislocations was not easily found. Dislocations appeared to have surfaced and disappeared from the grid like foil. Also if found then an uncertainty as to when were dislocations pinned existed (during hot compression or while TEM sample preparation). The objective was to search for precipitates and not the preservation of the dislocation arrangement, which is difficult on copper. On the copper samples where no precipitates were found then some features of general interest were captured, as can be seen on figures 3.76 and 3.77. Several images were taken, which might not be in the interest of searching for precipitates, but what should be emphasized is that precipitates were found in coppers with higher oxygen content after being in warm working temperatures.

Fig. 3.69 A bright field TEM image of Cu B after 750ºC, $0.3s^{-1}$ and $\varepsilon = 0.8$. The image only shows a flaky or grid like pattern.

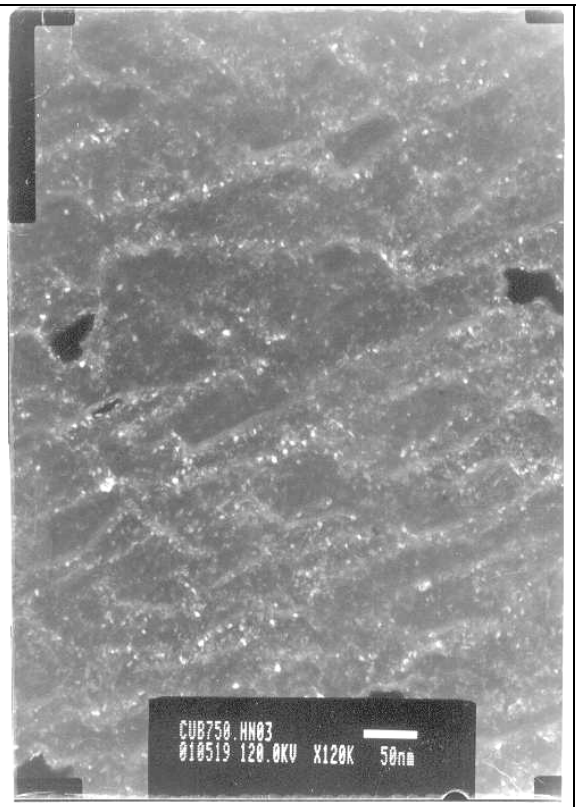

Fig. 3.70 Above is a dark field image of fig. 3.69, which shows white precipitates outlining the grid like pattern seen on previously.

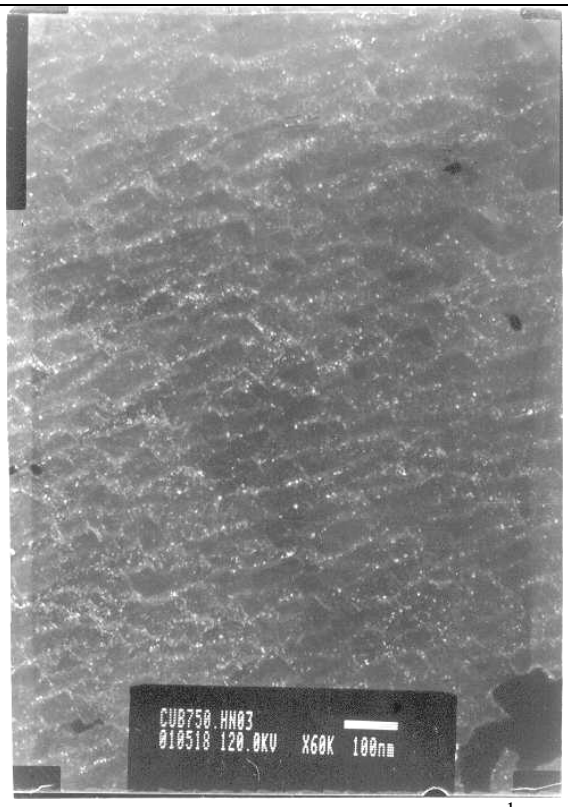

Fig. 3.71 Another dark field image of Cu B after 750ºC, $0.3s^{-1}$ and $\varepsilon = 0.8$, which shows the grid like structure adopted by the white precipitates.

A collage of images and corresponding electron diffraction patterns may help summarize the findings of the TEM investigation. Figure 3.78 shows the TEM images obtained from the samples compressed at 900ºC and $0.3s^{-1}$ (the three images above) and from the samples compressed at 750ºC and $0.3s^{-1}$ (the three images below). On the upper left hand corner of each image is a Selected Area Diffraction pattern, corresponding to the crystalline nature of the images. On fig. 3.78 images (e) and (f) are dark field images, which reveal in white the sources of the ring diffraction pattern, once focused. The bright spots are small crystalline particles of Cu_2O, which individually produce a diffraction pattern, but because each is oriented randomly many diffraction patterns are produced creating a ring diffraction pattern. As is known, another reason ring diffraction patterns form is when copper is deformed to large plastic strains and boundary misorientation becomes high [10], which is not the case for these TEM samples. Copper B tested at 750ºC revealed many rings on the diffraction pattern, which belong not only to the fine crystallites of Cu_2O but also to the copper matrix. As explained before the presence of precipitates makes the production of a smooth surface difficult, creating edges that can also diffract electrons corresponding to other planes of the copper matrix. Copper C tested at 750ºC revealed one clear ring on the diffraction pattern and other four faint rings. The diffraction spots belong to the copper matrix. The faint and blurry appearance of the rings on fig. 3.78 made characterization of the precipitate difficult.

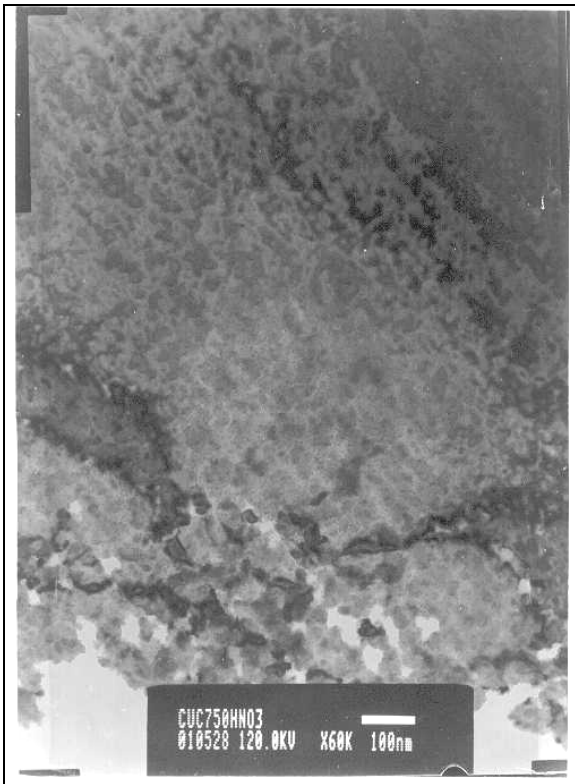

Fig. 3.72 A TEM bright field image of Cu C after 750ºC, $0.3s^{-1}$ and $\varepsilon = 0.8$. Through this mode precipitates are difficult to observe.

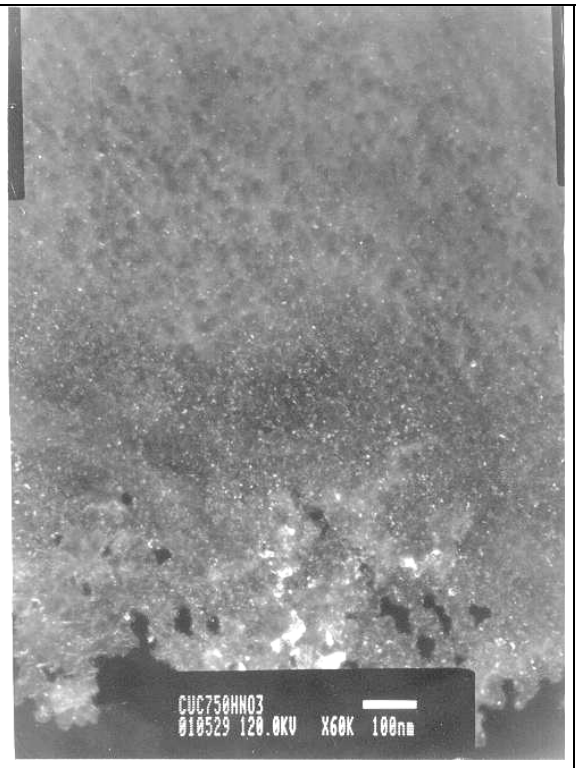

Fig. 3.73 A dark field image of fig. 3.72 Reveals several fine precipitates (in white).

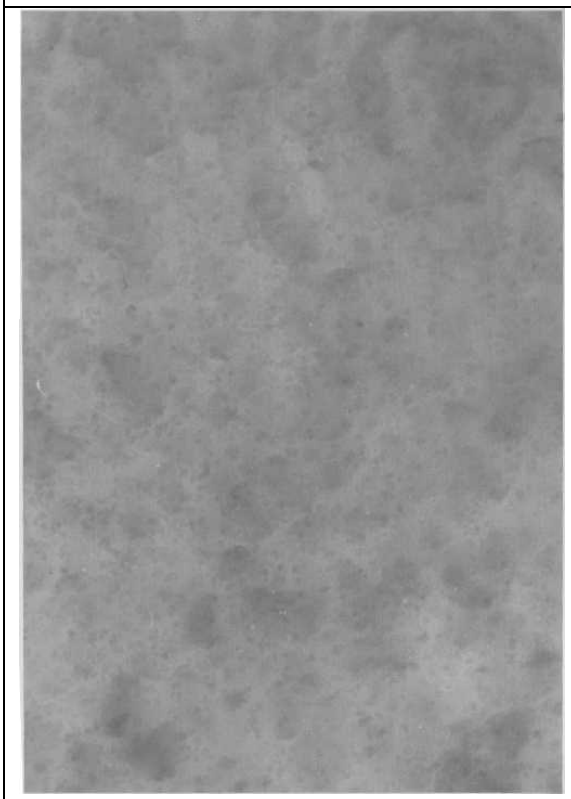

Fig. 3.74 A zoom of the bright field image on fig. 3.72. Precipitates are not easily viewed while on bright field mode.

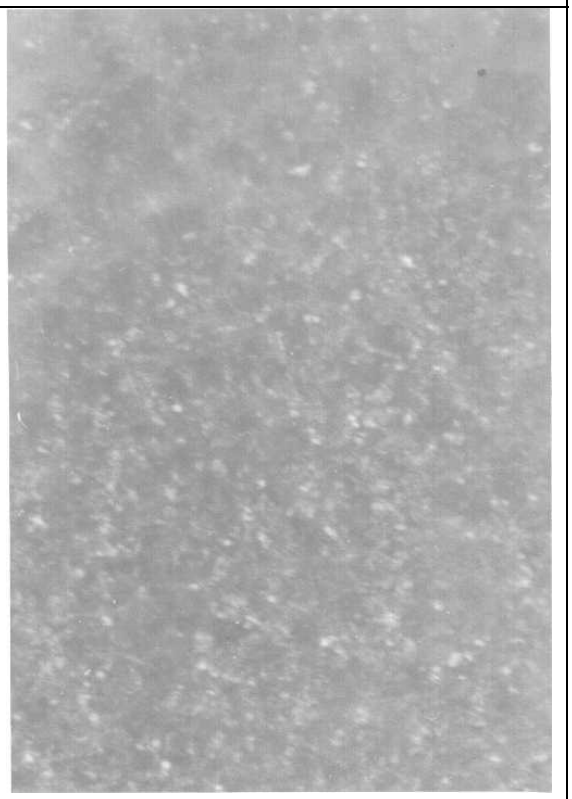

Fig. 3.75 A zoom of the dark field image on fig. 3.73. The white precipitates have an irregular shape.

Fig. 3.76 The TEM foils from compressed samples after 900ºC, $0.3s^{-1}$ and $\varepsilon = 0.8$ did not show any precipitates, only regular images like above from Cu B where a triple junction grain boundary is seen with dislocations in contrast.

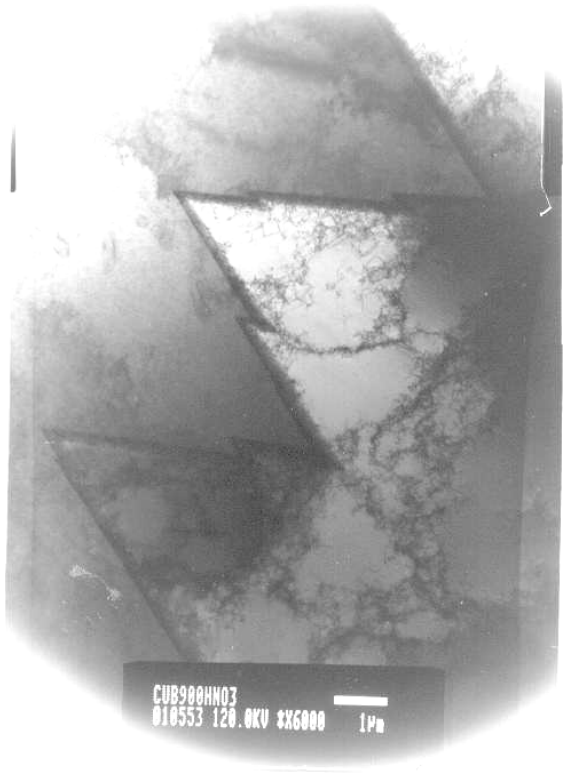

Fig. 3.77 The image above is another image of Cu B after being compressed at 900ºC. Above a semi-coherent and coherent twin boundaries were captured on the same image. Dislocations on one side are in contrast.

The characterization of the precipitate probably responsible for an increase in flow stress was done using a nanocrystalline Cu C sample. The TEM results from a sample of Cu C tested at 750ºC (see fig. 3.79) and prepared using the ion milling thinning technique revealed how many rings should form (copper plus precipitate rings). The ion milling thinning technique previously deforms the copper matrix at room temperature (when dimple grinding) and later the ion bombardment promotes static recrystallization producing a nanocrystalline structure. Other researchers have already reported the production of a nanocrystalline copper structure at room temperature [10]. Nanocrystalline copper has been viewed and studied by TEM [11], however powder metallurgy was employed to produce larger samples. Having the ring patterns of the known material (copper) mixed with the rings of the unknown precipitate allowed calibrating *in situ* the camera constant (λL) reducing the error when calculating the interplanar spacings d_n of the precipitate (see fig. 3.80). Many of the possible precipitates have similar interplanar spacings. The additional difficulty was overcome by the fact that the (111) plane, which diffracts with maximum intensity in Cu_20 [12], coincides with the ring of maximum intensity that did not belong to the copper matrix. TEM images in this study have showed the appearance of fine Cu_20 precipitates in the coppers with higher oxygen content when tested at the lower temperatures (0.64-$0.75T_h$), which also coincide with the appearance of an added back stress.

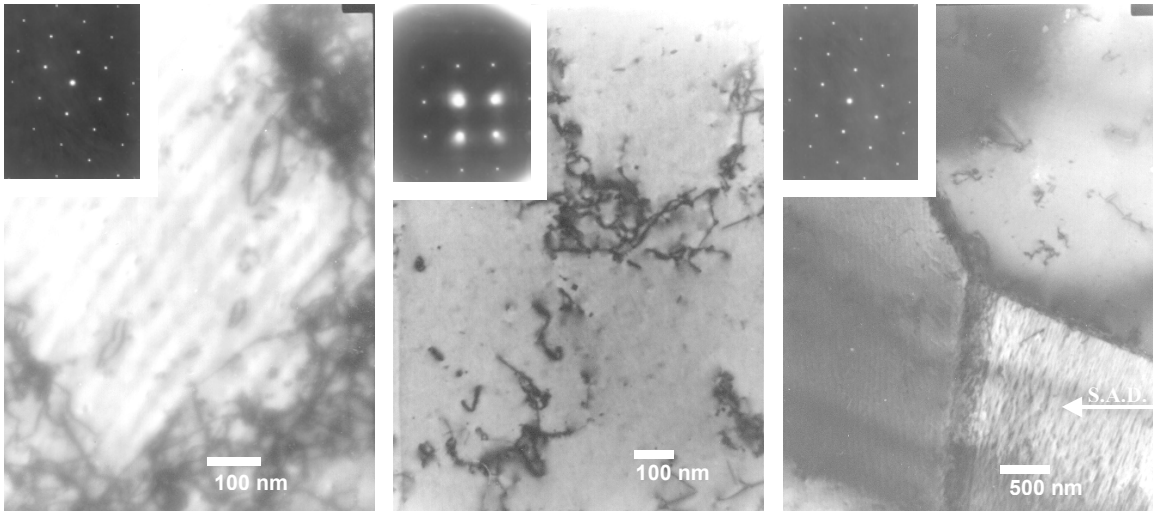

a) Cu A tested at 900ºC and $0.3s^{-1}$ presented a single diffraction pattern.

b) Cu B tested at 900ºC and $0.3s^{-1}$ presented a single diffraction pattern.

c) Cu C tested at 900ºC and $0.3s^{-1}$ presented a single diffraction pattern.

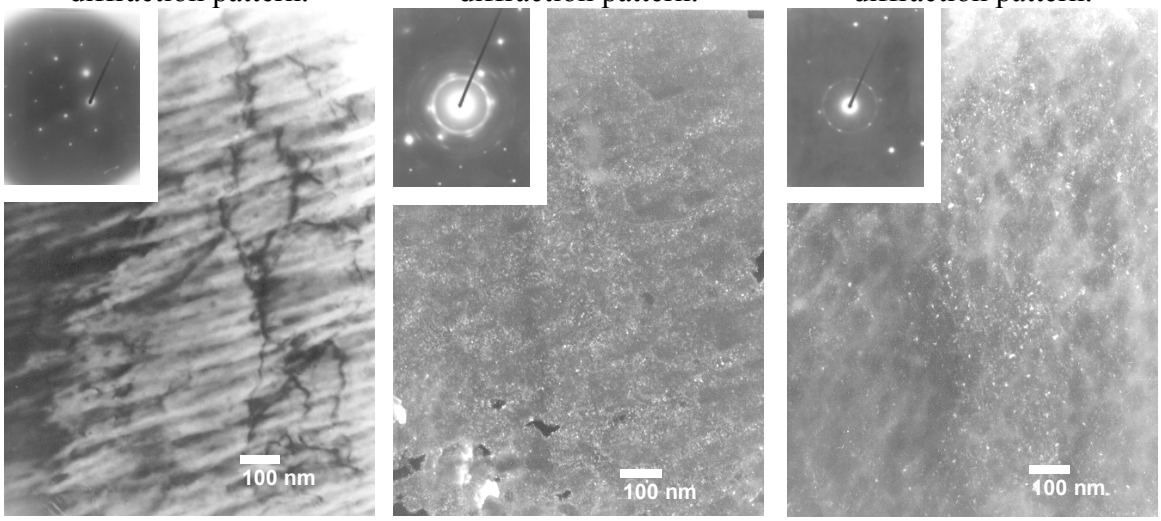

d) Cu A tested at 750ºC and $0.3s^{-1}$ presented a single diffraction pattern.

e) Cu B tested at 750ºC and $0.3s^{-1}$ presented a multiple ring diffraction pattern.

f) Cu C tested at 750ºC and $0.3s^{-1}$ presented a ring diffraction pattern.

Fig. 3.78 TEM images above resume the results obtained while searching for precipitates that might strengthen the copper matrix during warm working temperatures like 750ºC. The only fine precipitates found correspond to samples tested at 750ºC and higher oxygen content, i.e. Cu B and Cu C, seen on (e) and (f).

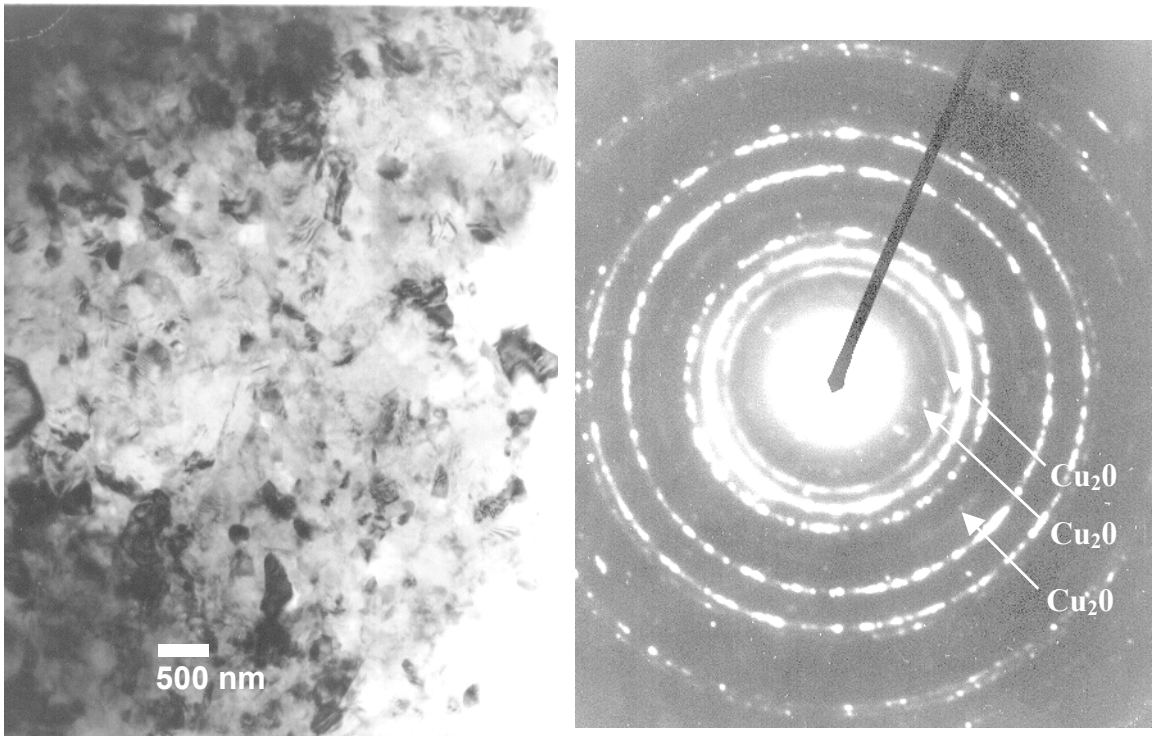

a) Nanocrystals of Cu C produced after dimple grinding and ion milling.

b) Multiple ring pattern of sample in (a).

Fig. 3.79 TEM images of Cu C tested at 750ºC and $0.3s^{-1}$ and then ion milled. The advantage of having produced nanocrystalline copper is that the ring pattern is more intense facilitating analysis unlike the ring pattern from fig 3.78 (e) and (f).

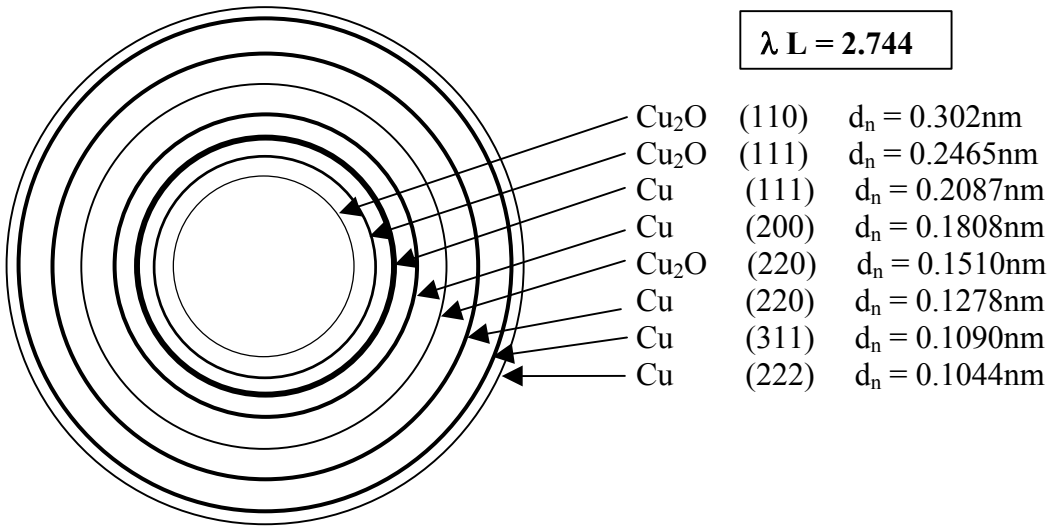

Fig. 3.80 Interplanar spacings d_n that match with correspondent diffraction rings of fig. 3.79.

3.6 Hardness of the Final Microstructure

The hardness of an annealed copper is approximately 40 to 45 VHN, but the hardness measurements of the hot compressed samples of Cu A, Cu B and Cu C showed that as the compression temperature was lower a higher hardness was produced. However ordered differences were found when comparing the three coppers. Figures 3.81, 3.82 and 3.83 show the Vickers hardness average values of the compressed samples versus strain rate for Cu A, Cu B and Cu C respectively. The hardness values are organized in lines according to the temperature of the hot compression tests. Each data point corresponds to the average of five indentations. On the three plots the samples compressed at 600ºC registered the highest hardness values. The second hardest samples correspond to the ones tested at 650ºC. The plots of two coppers with higher oxygen, Cu B and Cu C (figures 3.82 and 3.83), clearly show that the third hardest samples correspond to the 700ºC data line. On the latter figures the hardness values for temperatures higher than 700ºC mix in with the rest of the temperature lines. A behavior that can be observed only on Cu B and Cu C is that as the strain rate was faster the resulting hardness value was higher. The latter behavior is not observable on fig. 3.81 of Cu A probably because the quenching procedure allowed enough annealing time. However the most probable reason for the hump seen on the plots of 600ºC and 650ºC for Cu A is some precipitation of Cu_2O particles. The size and volume fraction precipitated produced only a minor hardening is compared to Cu B and Cu C. Another observation from the plots is that the lowest hardness values only in few occasions corresponded to the highest temperature of 950ºC. Again the quenching time could be introducing error. In any case a slight hardening of the microstructure seems to have happened even at 950ºC.

A hardness comparison between the coppers showed that the oxygen content was of influence especially in samples tested at lower temperatures (700ºC-600ºC). Plots that compare the three coppers at different temperatures are shown on fig. 3.84. In the plots of 600ºC, 650ºC and 700ºC where the scale is from 40 to 90 VHN, Cu C with the highest residual oxygen content produced a harder microstructure under the same warm working conditions. In the same plots Cu A with the lowest oxygen content was always the softest. On the plots of higher temperatures the scale is smaller, however with the exception of 800ºC and 850ºC a similar trend can be supposed. For example in the 950ºC plot the hardness values are all low, but a trend exists where Cu C is the hardest and Cu A the softest. The plots allow observing that the copper with higher oxygen will produce a harder final microstructure, especially after warm working temperatures. Bearing in mind the presence of precipitates an explanation to the observed hardness trend is that the size and volume fraction of precipitates increases the hardness of the final microstructure. A pure copper would still present a higher hardness as the forging temperature is lowered (and as the strain rate is higher), however no humps would appear and the hardness increment would be smaller. Higher oxygen levels in the coppers studied created increasingly more effective size and volume fraction of precipitates that helped block dislocation movement during indentation.

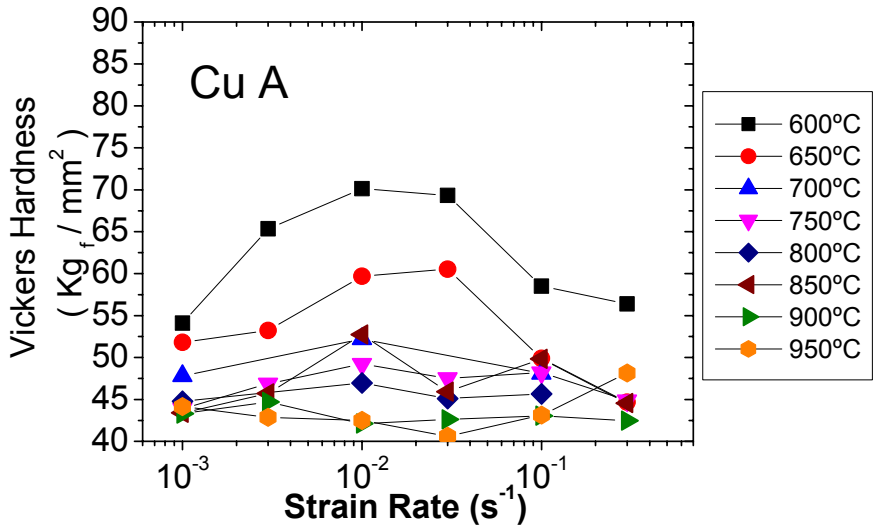

Fig. 3.81 The plot above shows the hardness of Cu A after hot forming to a strain of 0.8.

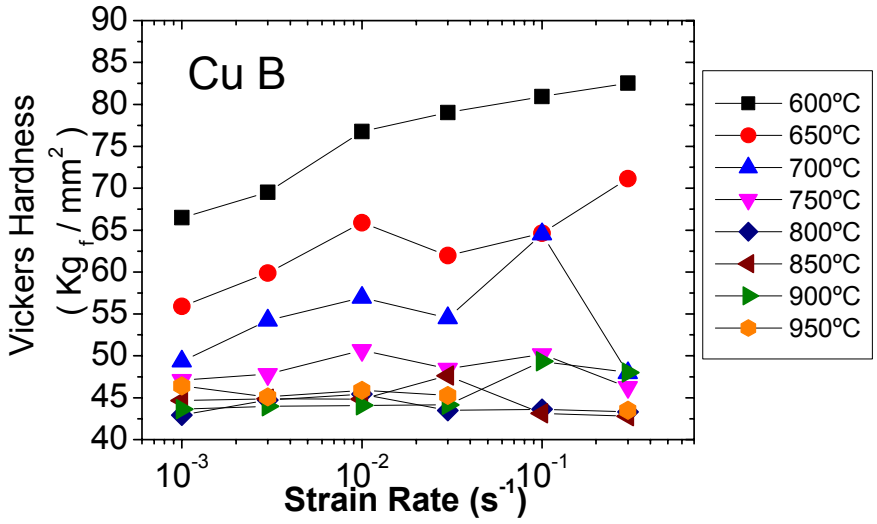

Fig. 3.82 The plot above shows the hardness of Cu B after hot forming to a strain of 0.8.

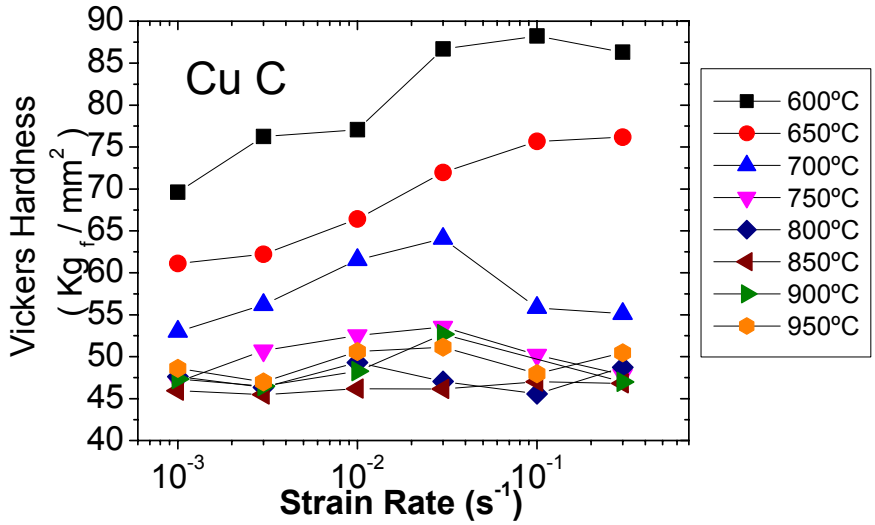

Fig. 3.83 The plot above shows the hardness of Cu C after hot forming to a strain of 0.8.

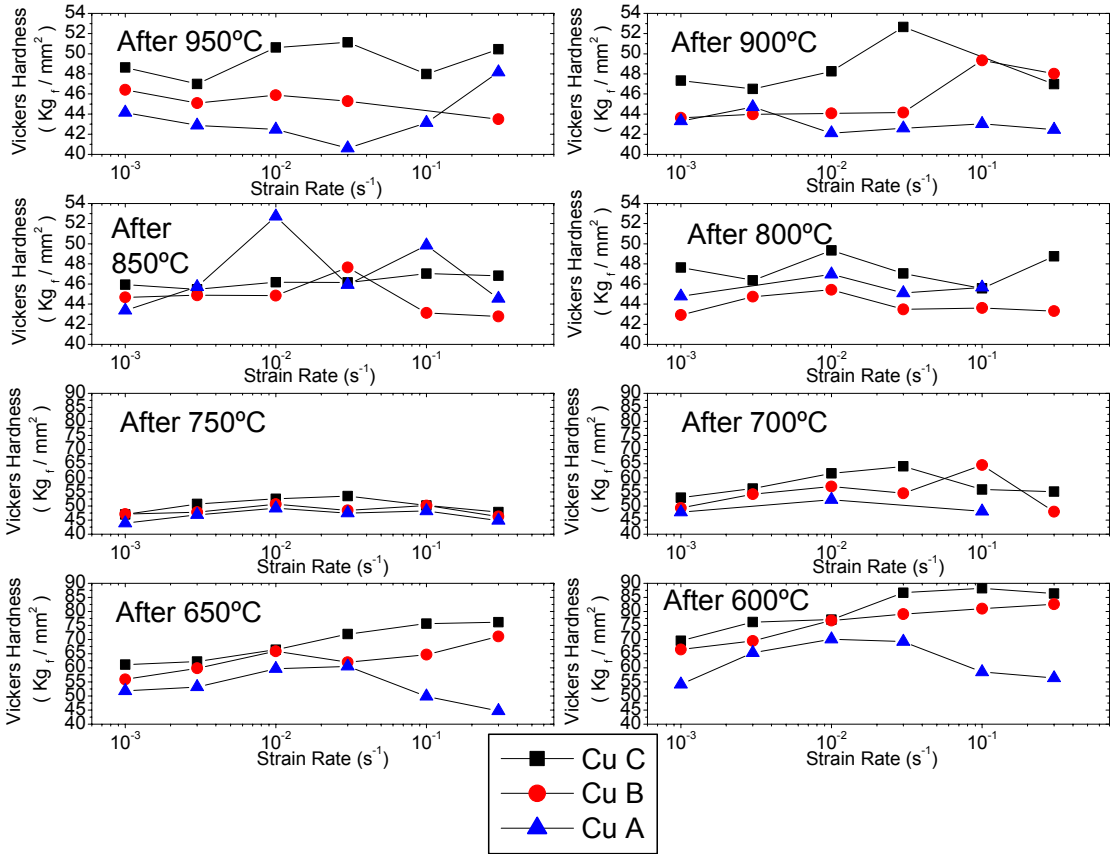

Fig. 3.84 A comparison of the Vickers hardness of the final microstructure between coppers A, B and C at different hot forming temperatures. At lower temperatures (700ºC-600ºC) copper C with the highest oxygen content produced a harder microstructure and copper A with the lowest oxygen content produced the softest microstructure. Notice that the hardness scale of the plots for 750ºC to 600ºC is larger.

3.7 References

[1] Archbutt S.L., Prytherch W.E., Effect of Impurities in Copper, British Non-Ferrous Metals Research Association, R. Clay & Sons Limited, Bungay, Suffolk, (1937), pp.1-135.

[2] Gao, W., Belyakov, A., Miura, H., Sakai, T., Dynamic Recrystallization of Copper Polycrystals with different impurities, Materials Science and Engineering, A265, (1999), pp. 233-239.

[3] Fujiwara, S., Abiko, K., Ductility of Ultra high Purity Copper, Journal de Physique IV, Colloque C7, supplément au Journal de Physique III, vol. 5, November 1995.

[4] Prasad Y.V.R.K., Rao K.P., Influence of Oxygen on Rate-Controlling Mechanisms in Hot Deformation of Polycrystalline Copper: Oxygen-Free Versus Electrolytic Grades, Material Letters 58, (2004), pp. 2061-2066.

[5] Prasad Y.V.R.K., Rao K.P., Mechanisms of High Temperature Deformation in Electrolytic Copper in Extended Ranges of Temperature and Strain Rate, Materials Science and Engineering, A 374, (2004), pp. 335-341.

[6] Wusatowska-Sarnek A.M., Miura H., Sakai T., Blackburn M.J., New Grain Formation under Dynamic Recrystallization of Copper, Proceedings of the First Joint International Conference on Recrystallization and Grain Growth (Aachen), Eds. Gottstein G. And Molodov D.A., Springer-Verlag, Berlin, vol.1, (2001), pp.899-904.

[7] Wusatowska-Sarnek A.M., Miura H., Sakai T., Nucleation and Microtexture Development Under Dynamic Recrystallization of Copper, Materials Science and Engineering A323 (2002) pp. 177-186.

[8] Rius I Grasset Anna, Garcia V., Cabrera J.M., Prado J.M., unpublished work.

[9] Edelson B.I., Baldwin JR. W.R., The Effect of Second Phases on the Mechanical Properties of Alloys, Transactions of the ASM, vol.55 (1962), pp. 230-250.

[10] Shih M.H., Yu C.Y., Kao P.W., Chang C.P., Microstructure and Flow Stress of Copper Deformed to Large Plastic Strains, Scripta Materialia 45 (2001), pp. 793-799.

[11] Youngdahl C.J., Weertman J.R., Hugo R.C., Kung H.H., Deformation Behavior in Nanocrystalline Copper, Scripta Mater. 44 (2001) pp. 1475-1478.

*[12] Swanson Howard E., Gilfrich Nancy T., Ugrinic George M., Standard X-ray Diffraction Powder Patterns, National Bureau of Standards Circular 539, Vol. II, Issued October 21, (1955), pp.1-75.